MITSUBISHI ELECTRIC RESEARCH LABORATORIES
https://www.merl.com

3D-Dynamic Safety Envelope-Based Control Strategy for Hyper-Redundant Manipulator Moving in Confined Space

Ju, Renjie; Zhang, Dong; Wang, Yebin; Zhou, Mengchu; Cao, Zhengcai

TR2026-105 July 03, 2026

Abstract

Hyper-redundant manipulators (HRMs) are used in non-invasive on-site maintenance tasks of aeroengines owing to their excellent dexterity and adaptability. However, it is challenging for them to achieve the obstacle avoidance planning in confined environment compared to conventional manipulators. This work presents a 3Ddynamic safety envelope (3DSE) based collision avoidance strategy to tackle this challenge. First, unlike conventional obstacle expansion-based methods that are computationally expensive and conservative, 3DSE is proposed and applied to establish collision constraints. Then, the motion in confined spaces is divided into trajectory tracking and blade detection processes. To address the issue of HRM's inability to fully track the trajectory, the continuous motion trajectory is discretized, and 3DSE is employed to update the trajectory nodes. The blade detection process when the base is fixed is modeled as an inverse kinematics (IK) problem of HRM, and a heuristic serpentine scanning method based on 3DSE and regional adaptation is proposed. An 18 degrees-of-freedom HRM prototype is built to experimentally validate the mechanical design and the performance of the proposed method. The results show that it well completes the traversing and fault detection of multistage blades in confined space.

IEEE Transactions on Industrial Electronics 2026

Mitsubishi Electric Research Laboratories, Inc.
201 Broadway, Cambridge, Massachusetts 02139

3D-Dynamic Safety Envelope-Based Control Strategy for Hyper-Redundant Manipulator Moving in Confined Space

Renjie Ju, Dong Zhang, *Member, IEEE*, Yebin Wang, *Senior Member, IEEE*
MengChu Zhou, *Fellow, IEEE*, and Zhengcai Cao, *Senior Member, IEEE*

***Abstract*—Hyper-redundant manipulators (HRMs) are used in non-invasive on-site maintenance tasks of aero-engines owing to their excellent dexterity and adaptability. However, it is challenging for them to achieve the obstacle avoidance planning in confined environment compared to conventional manipulators. This work presents a 3D-dynamic safety envelope (3DSE) based collision avoidance strategy to tackle this challenge. First, unlike conventional obstacle expansion-based methods that are computationally expensive and conservative, 3DSE is proposed and applied to establish collision constraints. Then, the motion in confined spaces is divided into trajectory tracking and blade detection processes. To address the issue of HRM's inability to fully track the trajectory, the continuous motion trajectory is discretized, and 3DSE is employed to update the trajectory nodes. The blade detection process when the base is fixed is modeled as an inverse kinematics (IK) problem of HRM, and a heuristic serpentine scanning method based on 3DSE and regional adaptation is proposed. An 18 degrees-of-freedom HRM prototype is built to experimentally validate the mechanical design and the performance of the proposed method. The results show that it well completes the traversing and fault detection of multistage blades in confined space.**

***Index Terms*—3D-Dynamic safety envelope, Hyper-redundant manipulator, obstacle avoidance.**

I. Introduction

COMPARED with conventional industrial manipulators, hyper-redundant manipulators (HRMs) demonstrate superior performance in navigating confined space due to their higher diameter-to-length ratio [1]. They facilitate an efficient and non-invasive solution for contactless operating tasks, e.g., detecting deep cavity of equipments [2], [3], assembling parts in a space station [4], and performing equipment maintenance in aero-engine and nuclear power plants [5], [6].

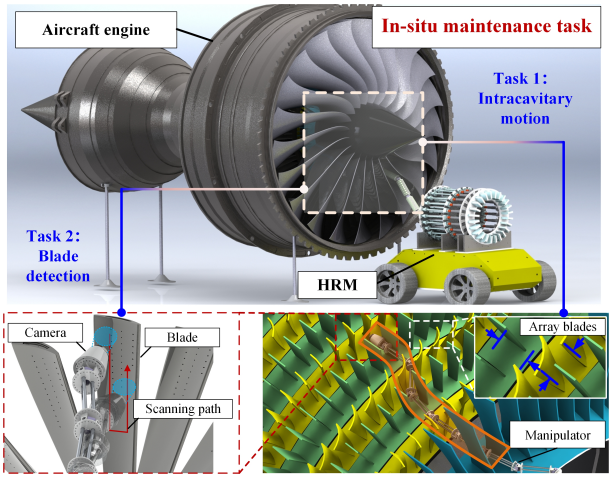

Fig. 1. HRM carries out a in-situ aero-engine maintenance task. It needs to traverse confined space and detect potential damage on blades.

In terms of their structures, HRMs can be roughly categorized into two types: continuum one and discrete one [7], [8]. A continuum HRM theoretically possesses an infinite number of degrees of freedom (DOFs). It is however impractical because not all DOFs can be activated in real-world applications. A discrete HRM offers greater accuracy and load capacity, owing to its rigid links and active revolute joints, which help prevent secondary damage during contactless operations [9], [10]. In our previous work [11], an 18-DOF cable-driven articulated HRM with a mobile platform was developed.

Fig. 1 shows an HRM which performs dexterous operations in a in-situ aero-engine maintenance task. First, HRM is navigated through the narrow space between blades to get close to the target pose, and then a blade detection process is performed by scanning. The main challenges include precise trajectory planning and tracking in confined environments, and performing blade scanning while avoiding obstacles. However, redundant DOFs present considerable challenges to achieve collision-free planning and control, owing to the complex nonlinearities and independent constraints. Moreover, the redundant DOFs leads to the curse of dimensionality, making it difficult to obtain feasible solutions in real time. Zhang et al. [12] propose a kinematic obstacle avoidance algorithm for space HRMs. Inspired by morphological methods, they apply

This work is supported in part by the National Key Research and Development Program of China under Grant 2024YFB4709100, in part by the National Natural Science Foundation of China 52535001 and 52475005, in part by the Aeronautical Science Foundation of China under Grant 2025L015077001. *(Corresponding authors: MengChu Zhou; Zhengcai Cao.)*

Renjie Ju and Dong Zhang are with the College of Information Science and Technology, Beijing University of Chemical Technology, Beijing 100029, China (e-mail: jurj@buct.edu.cn, zhang_dong@buct.edu.cn).

Yebin Wang is with Mitsubishi Electric Research Laboratories, Cambridge, MA 02139 USA (e-mail: yebinwang@ieee.org).

MengChu Zhou is with the Department of Electrical and Computer Engineering, New Jersey Institute of Technology, Newark, NJ 07102, USA (e-mail: zhou@njit.edu).

Zhengcai Cao is with the State Key Laboratory of Robotics and Systems, Harbin Institute of Technology, Harbin 150080, China (e-mail: caozc@hit.edu.cn).

rapidly exploring random tree algorithm for static obstacles and backbone curve fitting algorithm for dynamic obstacles. In [13], a motion planning algorithm based on the intersection of constraint manifolds and regions is proposed for redundant manipulators to avoid obstacles. Using a conditional generative adversarial network, their algorithm demonstrates generalization capability in similar scenarios without the need for retraining. Luo et al. [14] design a follow-the-leader algorithm with a two-level planner. Reinforcement learning method is applied to obtain a collision-free trajectory in local planner by optimizing parameters, e.g., target error, angle deviation, and tension equalization. An observation tree is applied by the global planner to optimize path nodes. A key limitation of these methods is the lack of guidelines for selecting obstacle expansion dimensions. Although intended to ensure a safe distance, this method directly infringes upon HRM's free workspace, leading to planning failure.

At the control level, various trajectory tracking methods are proposed to ensure that HRMs follow the collision-free trajectory and reduce tracking errors. Mohammad et al. [15] design a follow the-leader strategy combined with an error minimization method for the evaluation of the optimal configuration of a single section. Work [16] proposes a prediction lookup and interpolation algorithms by optimizing discrete interpolation points to reduce tracking errors. Jiang et al. [17] design a sliding mode and a nonlinear disturbance observer using linear matrix inequality to reduce tracking errors and achieve full-body trajectory tracking. Although some work have investigated the deviation during trajectory tracking process [18], limited numerical analysis has been conducted.

During the blade detection process, the end precision of HRM is enhanced by fixing the base. The motion control of HRM is modeling as an inverse kinematics (IK) problem. Zhou et al. [19] propose a pitch-free backbone curve-based IK method to describe the movement of snake robots with multiple rolling joints. In [20], a spatial tri-arc planning method is proposed. By adjusting the shape of the spatial tri-arc, the IK problem of a manipulator is simplified to a curve fitting problem. Xu et al. [21] present an IK method based on the morphologic space constraints. Their method directly obtains positions of links in configuration space to improve calculation efficiency, rather than solving in joint space. The precise guidance of HRM's end-effector along a complex trajectory within a constrained workspace remains a fundamental challenge, despite the existence of numerous IK solutions.

Although various collision avoidance control methods have been developed, it is difficult for HRMs to complete maintenance in narrow and tortuous space. There are two key challenges to be addressed:

1) Conventional path planning algorithms typically require obstacle inflation. In confined environments, excessive expansion of obstacles significantly reduces the available workspace, often leading to planning failure.
2) When distal joints perform scanning tasks within a narrow environment, it is crucial to minimize changes in joint space while satisfying the requirements of end-effector posture and obstacle avoidance.

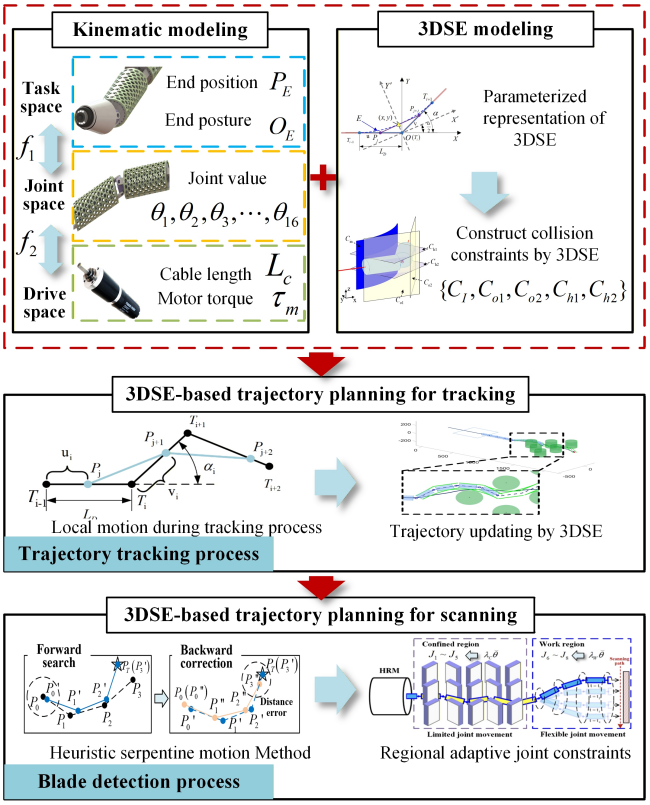

Fig. 2. Overall framework design of our work.

This work addresses these challenges and makes the following contributions:

1) propose a 3D-dynamic safety envelope (3DSE) method to avoid the excessive occupation of free space incurred by obstacle expansion treatment;
2) develop a 3DSE-based trajectory generation method for the HRM to navigate through narrow space during the tracking process;
3) design a 3DSE-based heuristic serpentine scanning method with regional adaptation to avoid secondary damage caused by collisions during the scanning process;
4) conduct extensive simulations and experiments by using a 18-DOF HRM.

The rest of this article is organized as follows. Section II presents the overall framework design of our work. In this part, HRM's kinematics model is established and 3DSEs are proposed to construct collision constraints. Section III applies 3DSE to achieve collision-free control of HRM during the trajectory tracking process and blade detection process. Numerical simulations and experiments are implemented in Section IV. Finally, Section V concludes the article and discusses our limitations and future work plan.

II. Problem Formulation and HRM System Modeling

A. Problem Formulation

To provide a clear understanding of our work, the overall framework diagram is presented in Fig. 2, which outlines the main components of our proposed control strategy and their interactions. It consists of the following key modules:

TABLE I
MATHEMATICAL SYMBOLS

Symbol	Description
$\{B\}$,$\{E\}$	Local reference coordinate system
L_d	Length of modular link
θ_i	Angles of Joint i
q_i	Position of Joint i
Θ	Configuration of HRM
P_jP_{j+1}	Link j
E	Envelope raised by HRM's link
T_n	Path nodes
α	Deviation angle of trajectory

1) The kinematic modeling module defines the pairwise mapping relationships between HRM's task space, joint space, and drive space (f_1 and f_2). It establishes the configuration and motion constraints of HRMs for the subsequent modules.
2) The 3DSE construction module establishes a safety area and evaluates collision risks based on trajectory tracking deviations. It comprises the parameterized representation and the obstacle avoidance constraint.
3) The trajectory tracking module decomposes the continuous motion of HRM into local movements between path nodes based on a sliding window method. By applying 3DSE to update joint nodes and optimize the trajectory, the obstacle avoidance capability of HRM in confined spaces is improved.
4) The blade scanning module models the motion of HRM with fixed base as an IK problem. A heuristic scanning method, integrating 3DSE and adaptive joint constraints, is proposed to derive the collision-free trajectory in the configuration space.

Mathematical symbols used in this manuscript are described in Table. I.

B. Kinematic Modeling

Fig. 3 illustrates an HRM where a manipulator with 8 active universal joints is mounted on a differential wheeled platform. The manipulator and the differential wheeled platform have 16-DOFs and 2-DOFs, respectively. The kinematic modeling consists of derivation of two mapping f_1 and f_2, where the former maps the configuration in joint space to the end posture in task space, and the latter maps the cable length in driving space to rotational angles in joint space.

We apply a product-of-exponentials (POE) method [22] to establish the kinematic model. Base frame is defined as $\{B\}$ and end-effector frame is defined as $\{E\}$.

1) Derivation of f_1: POE parameters for the HRM are provided in Table. II. w_i represents the unit direction vector associated with each axis, while q_i indicates the joint position in reference frame $\{B\}$. The joint twist is a 4×4 matrix and constructed by

$$\hat{\xi}_i = \begin{bmatrix} \hat{w}_i & v_i \\ 0_{1\times 3} & 0 \end{bmatrix}, \tag{1}$$

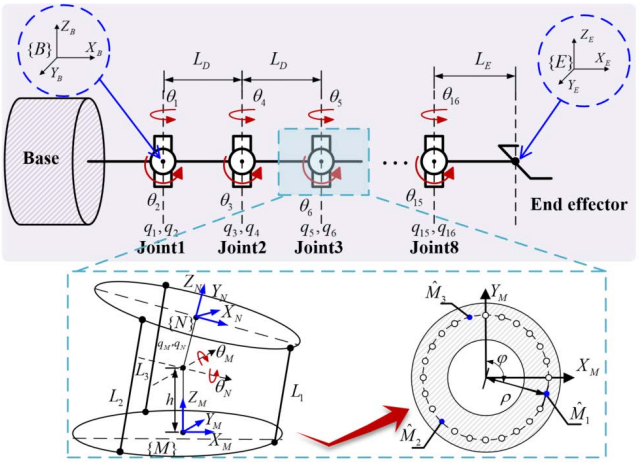

Fig. 3. Kinematic modeling of HRM.

TABLE II
POE PARAMETERS OF THE HRM

Index	w_i	q_i
1	$[0;0;1]$	$[0;\ 0;\ 0]$
2	$[0;1;0]$	$[0;\ 0;\ 0]$
3	$[0;1;0]$	$[L_D;\ 0;\ 0]$
4	$[0;0;1]$	$[L_D;\ 0;\ 0]$
$\vdots$	$\vdots$	$\vdots$
15	$[0;1;0]$	$[7L_D;\ 0;\ 0]$
16	$[0;0;1]$	$[7L_D;\ 0;\ 0]$

where $\hat{w}_i = \begin{bmatrix} 0 & -w_3 & w_2 \\ w_2 & 0 & -w_1 \\ -w_2 & w_1 & 0 \end{bmatrix}$ denotes the skew-symmetric matrix corresponding to w_i, and $v_i = -w_i \times q_i$ is linear velocity. Given a joint twist $\hat{\xi} \in^{4\times4}$ and the angular displacement $\theta \in \mathbb{R}$, the exponential product $e^{\hat{\xi}\theta}$ denotes the movement of HRM.

For the 16-DOFs HRM, let $\Theta \triangleq \{\theta_1, \theta_2, \ldots, \theta_{16}\}$ denote its configuration, and the corresponding twists for all joints are constructed as $\{\hat{\xi}_1, \ldots, \hat{\xi}_{16}\}$. Without loss of generality, the initial configuration of the HRM is set to $\Theta = 0_{1\times16}$. The initial configuration of the end-effector, represented in the base frame $\{B\}$, is denoted by the homogeneous transformation matrix $T_{B,E}(0) \in^{4\times4}$. Given an arbitrary configuration Θ, the configuration of the frame $\{E\}$, represented in the base frame, can be computed by the POE as follows:

$$\begin{aligned} f_1(\Theta) &= T_{B,E}(\Theta) \\ &= e^{\hat{\xi}_1\theta_1} e^{\hat{\xi}_2\theta_2} e^{\hat{\xi}_3\theta_3} \ldots e^{\hat{\xi}_{16}\theta_{16}} T_{B,E}(0), \end{aligned} \tag{2}$$

2) Derivation of f_2: The motor's rotation is transformed into the linear displacement of driving cables by screws. Then, the mapping from cable length in driving space to rotational angles in joint space should be established. As shown in Fig. 3, the reference frame located on two disks are defined as $\{M\}$ and $\{N\}$. The POE parameters of two rotational axes, which intersect at the center of mass (CM) of joints, are $w_M = [0;\ 1;\ 0]$, $\omega_N = [1;\ 0;\ 0]$ and $q_M = q_N = [0;\ 0;\ h]$. Then,

we have:

$$T_{M,N}(0) = \begin{bmatrix} 1 & 0 & 0 & 0 \\ 0 & 1 & 0 & 0 \\ 0 & 0 & 1 & 2h \\ 0 & 1 & 0 & 1 \end{bmatrix}, \tag{3}$$

where h is the euclidean distance between joint's CM and disk's CM. The transformation matrix $T_{M,N}(\theta_M, \theta_N)$ are:

$$\begin{aligned} T_{M,N}(\theta_M, \theta_N) &= e^{\hat{\xi}_1 \theta_M} e^{\hat{\xi}_2 \theta_N} T_{M,N}(0) \\ &= \begin{bmatrix} C_M & S_M S_N & S_M C_N & h S_M C_N \\ 0 & C_N & -S_N & -h S_N \\ -S_M & C_M S_N & C_M C_N & h + h C_M C_N \\ 0 & 0 & 0 & 1 \end{bmatrix}, \end{aligned} \tag{4}$$

where $C_M = \cos\theta_M$, $S_M = \sin\theta_M$, $C_N = \cos\theta_N$, and $S_N = \sin\theta_N$. θ_M and θ_N are the pitch and yaw angles of local joint.

The positions of cables' endpoints $\hat{M}_i$ and $\hat{N}_i$ in the reference frame $\{M\}$ are:

$$\begin{aligned} \hat{M}_i &= \begin{bmatrix} \rho C_\varphi, & \rho S_\varphi, & 0, & 1 \end{bmatrix}^T, \\ \hat{N}_i &= T_{M,N} \hat{M}_i, i \in \{1, 2, 3\}, \end{aligned} \tag{5}$$

where ρ represents the euclidean distance between CM and the corresponding cable hole. The cable length can be computed according to the desired rotation angles as:

$$\begin{aligned} L(\theta_M, \theta_N, \varphi) &= \|\hat{N}_i - \hat{M}_i\| \\ &= ((\rho C_\varphi (C_M - 1) + h S_M C_N \\ &+ \rho S_\varphi S_M S_N)^2 + \rho S_\varphi (C_N - 1) - h S_N)^2 \\ &+ (h(C_M C_N + 1) - \rho C_\varphi S_M \\ &+ \rho S_\varphi C_M S_N)^2)^{\frac{1}{2}}. \end{aligned} \tag{6}$$

III. Main Results

The construction of a collision constraint model for HRMs in confined environments with multiple obstacles presents a significant challenge. This paper introduces the concept of 3DSE for the first time to assess collision risks and demonstrates the results on a 18-DOFs HRM.

A. 3DSE modeling method

Due to the structural characteristic of HRM, it is unable to fully track the reference trajectory . Thus, the area resulting from HRM's deviation from the reference trajectory must be considered to establish obstacle avoidance constraints. It is interesting that the envelope line in mathematical theory can be used to study trajectory deviation problems [23]. However, there lack studies addressing the external envelope of the collision areas of HRMs. In this part, a 3DSE is proposed for the first time and undergoes parametric analyses.

As shown in Fig. 4(a), envelope E is generated by the sliding motion of Link P_jP_{j+1} at the path nodes T_{i-1}, T_i and T_{i+1}. The deflection angle among three path nodes is denoted as α. Notably, the relevant calculation is performed on the plane formed by three adjacent path nodes. The motion of 2-DOFs joint is approximated as a rotation of angle α around a specific axis in space.

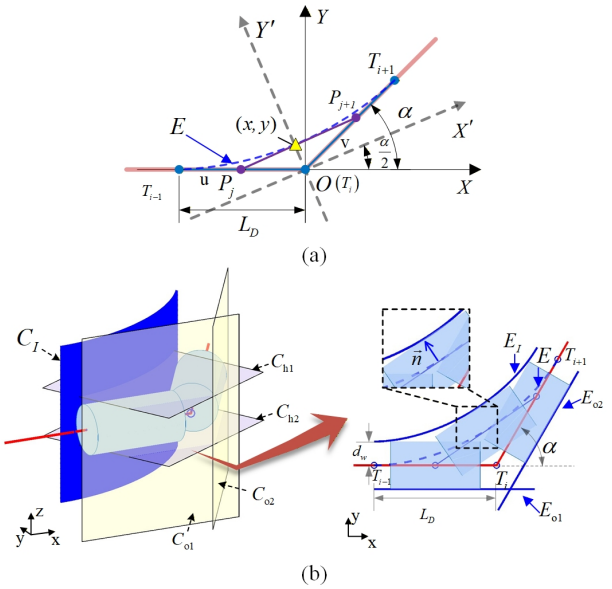

Fig. 4. Illustration of geometric approach for 3DSE. (a) Parameterized representation of simplified model. (b) Envelope surface constraint established by actual link.

According to the concept of line family in mathematics [24], each line in the family P_jP_{j+1} is tangent to E at point (x, y). The frame $\{X'OY'\}$ is designed to simplify the calculation, with $\angle X'OX = \frac{\alpha}{2}$. In the frame $\{XOY\}$, we assume the coordinates of the joint j endpoints $P_j(u, 0)$ and $P_{j+1}(v\cos\alpha, v\sin\alpha)$, where $u = \left|\overrightarrow{T_{i-1}P_j}\right|$ and $v = \left|\overrightarrow{OP_{j+1}}\right|$. Then, we have $P'_j(u\cos\frac{\alpha}{2}, -u\sin\frac{\alpha}{2})$ and $P'_{j+1}(v\cos\frac{\alpha}{2}, v\sin\frac{\alpha}{2})$ in the frame $\{X'OY'\}$. $G(x', y', v)$ is characterized as a family of lines, parameterized by u and v. Via line segment $P'_jP'_{j+1}$, it can be obtained:

$$G(x', y', v) = -\frac{x' - u\cos\frac{\alpha}{2}}{v\cos\frac{\alpha}{2} - u\cos\frac{\alpha}{2}} + \frac{y' + u\sin\frac{\alpha}{2}}{v\sin\frac{\alpha}{2} + u\sin\frac{\alpha}{2}}, \tag{7}$$

where $(u + v)^2 = 1 + 4uv\cos^2\frac{\alpha}{2}$. E can be obtained via:

$$\begin{cases} G(x', y', v) = 0 \\ \dfrac{\partial G(x', y', v)}{\partial v} = 0 \end{cases}. \tag{8}$$

Via (7) and (8), E in $\{X'OY'\}$ is obtained:

$$\begin{cases} x' = L_D(v + u)\cos\dfrac{\alpha}{2}(1 - 2uv\sin^2\dfrac{\alpha}{2}) \\ y' = L_D(v - u)\sin\dfrac{\alpha}{2}(1 + 2uv\cos^2\dfrac{\alpha}{2}) \end{cases}. \tag{9}$$

Therefore, E in $\{XOY\}$ is obtained:

$$\begin{cases} x = L_D v\cos\alpha + \dfrac{1}{2}L_d u(2 - v^2 + v^2\cos 2\alpha) \\ y = L_D v(1 - u^2 + uv\cos\alpha)\sin\alpha \end{cases}. \tag{10}$$

Considering the actually size of HRM's links, 3DSE is generated as shown in Fig. 4(b). From the top view, 3DSE is composed of inner envelope E_I and outer envelopes E_{o1} and E_{o2}. The radius of HRM's link is d_w. E_{in} is generated by translating the tangent point along the normal vector $\vec{n}$ by distance d_w. Respectively, E_{o1} and E_{o2} are parallel to the corresponding reference trajectories $\overrightarrow{T_{i-1}T_i}$ and $\overrightarrow{T_iT_{i+1}}$.

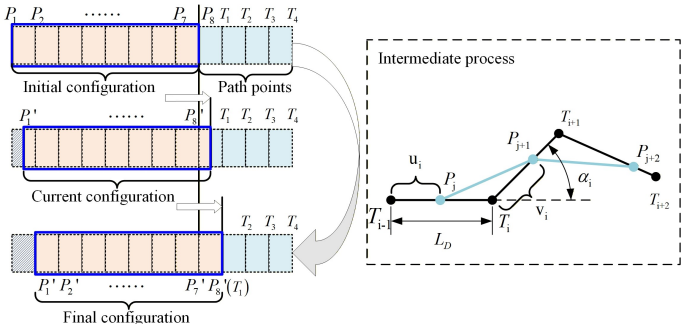

Fig. 5. Model of local motion during the tracking process.

To further apply 3DSE to avoid obstacles, complete obstacle avoidance constraints are defined as composition of internal envelope surface constraint C_I, external envelope surface constraints C_{o1} and C_{o2} , as well as height constraints C_{h1} and C_{h2}. By establishing a local reference frame, 3DSE can be expressed as:

$$\begin{cases} C_I = G(x,y,z) + d_w \\ C_{o1} = \{(x,y,z))|y + d_w > 0\} \\ C_{o2} = \{(x,y,z))|\sin\alpha x - \cos\alpha y - d_w < 0\}, \\ C_{h1} = \{(x,y,z))|z - d_w < 0\} \\ C_{h2} = \{(x,y,z))|z + d_w > 0\} \end{cases} \tag{11}$$

where $G(x,y,z)$ is the corresponding implicit equation of (10).

B. 3DSE-based trajectory planning for tracking

Detection tasks of equipment require HRMs to continuously traverse narrow environment without collisions with internal components. The discrete structure of HRMs hinders their ability to fully track reference trajectories, posing a heightened risk of collisions. To solve these problems, we propose a 3DSE based trajectory planning method for tracking.

1) Trajectory discretization: During the tracking process, the configuration of a manipulator is guided by the position and posture of the end joint, indicating that the remaining joints move in accordance with the end joint. To follow the movement mentioned, a sliding window model is integrated into the trajectory tracking strategy to describe local motion process between path points.

As shown in Fig. 5, HRM motion is discretized into individual motion primitives by path points. The intermediate processes within motion primitives are represented by sliding windows. The proportion of window between adjacent path nodes represents the completion degree of HRM's local motion between these nodes.

Continuous trajectories should be discretized to obtain path nodes.The reference trajectory $\hat{T}$ can be obtained by our previous trajectory planning method [25]. In this method, rapidly-exploring random trees (RRT) algorithm with probabilistic completeness and angle constraints is used to rapidly plan feasible paths, ensuring that HRM can accomplish its task. A* algorithm is adopt to evaluate the path cost. $P_1, P_2, \ldots,$ and P_8 are joint nodes of HRM. $\{P_1, P_2, \ldots, P_8\}$ represents

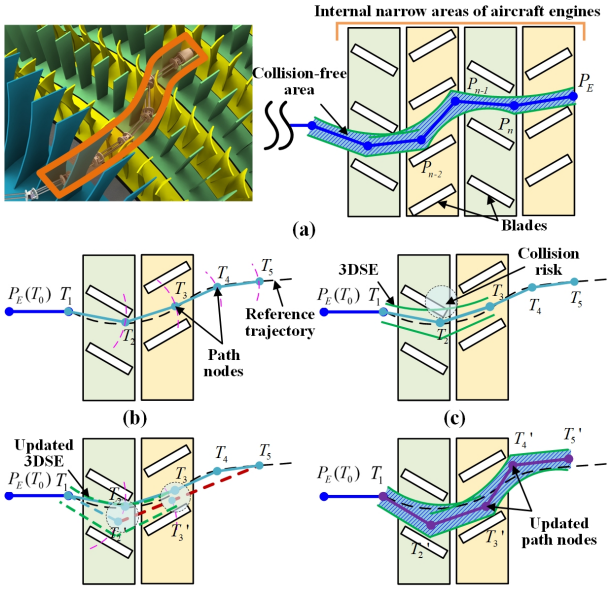

Fig. 6. 3DSE-based collision-free trajectory update strategy. (a) Overall schematic diagram. (b) Finding path nodes through interpolation search method. (c) Generating 3DSE and evaluating collision risk. (d) Updating path nodes. (e) Finding collision-free trajectory.

its current configuration. $T_0, T_1, T_2, \ldots,$ and T_k are discretized path points that should satisfy:

$$\begin{aligned} &\|T_i - T_{i-1}\| - L_d = 0 \\ &s.t. \quad T_i \in \hat{T}, i = 1, 2, 3, \cdots, k, \end{aligned} \tag{12}$$

where k is the number of path nodes. The euclidean distance between each pair of path nodes is equal to L_D. The current posture of joint j can be described as:

$$\begin{cases} \vec{\bar{P}_j P_{j+1}} = L_d(1-u_i)\vec{\bar{T}_{i-1}\bar{T}_i} + L_d v_i \overrightarrow{T_i T_{i+1}} \\ \alpha_i = \arccos \dfrac{\vec{\bar{T}_{i-1}\bar{T}_i} \cdot \overrightarrow{T_i T_{i+1}}}{|\vec{\bar{T}_{i-1}\bar{T}_i}||\overrightarrow{T_i T_{i+1}}|} \end{cases}, \tag{13}$$

where u_i and v_i are the interpolation coefficients and $\overrightarrow{P_j P_{j+1}}$ represents the vector of link j during the sliding process, while α_i represents the spatial relationships among three adjacent path points T_{i-1}, T_i and T_{i+1}.

2) Trajectory nodes update strategy: As shown in Fig. 6, we aim to improve the success rate of trajectory planning significantly in constrained space without performing obstacle expansion. According to the obstacle status, we apply 3DSE to evaluate collision risk and update path nodes. Our goal is to obtain collision-free trajectory composed of updated path nodes T_0', T_1', ..., and T_k'.

The whole 3DSE-based collision-free trajectory update strategy for HRM is realized in Algorithm 1.

Firstly, the initial path nodes $T_0, T_1, ...,$ and T_q are obtained via (12) according to a pre-planned trajectory where q is the number of the searched nodes, as shown in Fig. 6(b). T_0 coincides with point P_E. As shown in Fig. 6(c), 3DSE is calculated based on adjacent three path nodes T_0, T_1 and T_2. Once there exists a risk of collision with the blades, the path nodes should to be updated. The update rule of path nodes is shown in Fig. 6(d). By setting T_0 as the circular center, its adjacent node T_1 is rotated outward from the collision area by

Algorithm 1: 3DSE-based trajectory update algorithm.

Input: Reference trajectory T_r: T_0, T_1, ..., and T_k, current configuration of HRM $\{P_1, P_2, ...,$ and $P_n\}$, target position P_T, position of obstacles P_o, maximum number of iterations I_m, convergence threshold D, search interval of deviation angle $\delta\theta$, search step size q

Output: Collision-free trajectory T_r': T_0', T_1', ..., and T_k'

Initialize the step number $i = 0$;
Calulate current distance between target and HRM's end-effector via: $d_{et} = \left|\overrightarrow{P_n P_T}\right|$;
while $d_{et} < D$ **do**
  $t = 0$, $\breve{\theta} = 0°$;
  Via sliding window-based method and (12), obtain the path nodes T_i, T_{i+1}, ..., and T_{i+q} ;
  Generate 3DSE E_i of T_i, T_{i+1}, and T_{i+2} via (10)-(11);
  Check collision between E_i and P_o via (11) ;
  if *Collision occurs* **then**
    while $t < I_m$ **do**
      Update T_{i+1} by joint rotation $\breve{\theta}$ with rotational radius L_D and obtain T_{i+1}';
      Update T_{i+2} via (14) and obtain T_{i+2}';
      Recheck collision risk via (11);
      $t = t + 1$, $\breve{\theta} = \breve{\theta} + \delta\theta$;
    end
  end
  $d_{et} = \left|\overrightarrow{T_{i+2}' P_T}\right|$, $i = i + 1$;
end
Return T_0', T_1',...and T_k'.

deviation angle $\breve{\theta}$, maintaining a rotational radius L_D. After updating node T_1 into T_1', we update T_2 such that T_2' can lie on line segment $T_1' T_q$:

$$T_2' = (1 - \frac{L_d}{\left|\overrightarrow{T_1' T_q}\right|})T_1' + \frac{L_d}{\left|\overrightarrow{T_1' T_q}\right|} T_q. \tag{14}$$

In the same vein, the remaining path nodes are updated. As shown in Fig. 6(e), through a sequential optimization process, a collision-free trajectory is obtained.

Compared to existing expanded obstacles based methods [12], [13], our approach focuses on 3DSE-based obstacle avoidance post-processing in a narrow area. 3DSE-based strategy can quickly obtain paths and perform dynamic corrections. The entire process is based on spatial geometric rules for path point interpolation and updating. Therefore, our method has the same computational complexity as traditional path planning methods and does not require a complex iterative optimization process.

C. 3DSE-based trajectory planning for scanning

Once HRM successfully passes through confined regions, it initiates a scan of the target blade to detect any potential

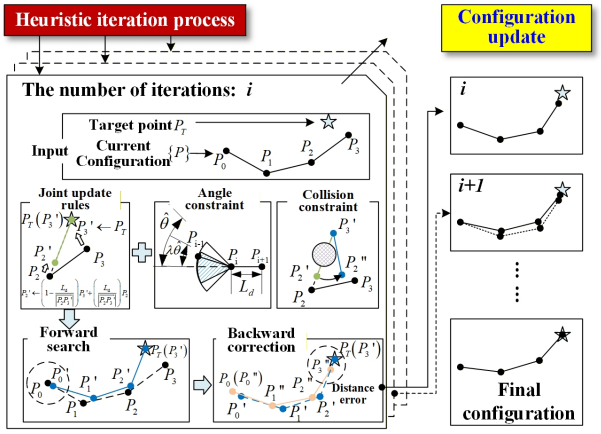

Fig. 7. Heuristic serpentine scanning.

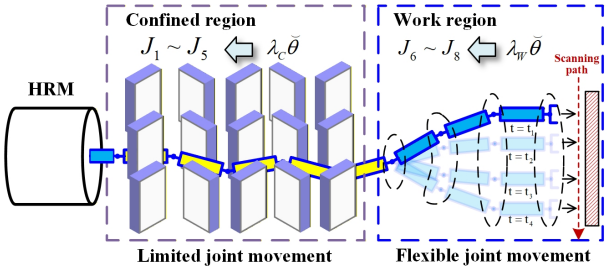

Fig. 8. Regional adaptive weight for HRM.

damage. The end-effector should move along a pre-defined path by adjusting the HRM joints while all the links of the HRM remains collision-free. The motion planning of HRM can be posed as an IK problem.

1) Heuristic serpentine motion method: To perform a comprehensive scan of the blade, it is crucial to minimize changes in joint space while satisfying the end-effector posture constraints and 3DSE-based collision constraints. Thus, we propose a heuristic serpentine scanning method based on 3DSE.

The existence of redundant DOFs makes it extremely difficult to establish its accurate mathematical model. There are numerous possible configurations for HRM to reach a given scanning position. As shown in Fig. 7, a heuristic method is applied to establish conversion rules among configurations and obtain the IK solution.

In this example, a three-link manipulator is demonstrated, with key input parameters including the initial configuration $\{P_0, P_1, P_2, P_3\}$ and the target P_T. During the iteration process, the configuration is updated to bring P_3 closer to P_T. The joint update rules are defined as:

$$\begin{cases} P_3' = P_T, \\ P_2' = (1 - \dfrac{L_d}{|\overrightarrow{P_2 P_3}|})P_3' + (\dfrac{L_d}{|\overrightarrow{P_2 P_3}|})P_2, \end{cases} \tag{15}$$

where P_2' and P_3' are updated joint nodes.

During the forward search process, P_3 moves to P_T and the rest joints are updated by joint update rules. As shown in Fig. 7, a new configuration $\{P_0', P_1', P_2', P_3'\}$ is computed. In the backward correction process, P_0' moves to P_0 to ensure that the base of HRM remains fixed. In the same way, the configuration $\{P_0'', P_1'', P_2'', P_3''\}$ is obtained. After a complete

iteration, the HRM's configuration is updated, and a distance error remains between its end-effector and the target P_T. Since the iterative process involves the update of joint nodes, 3DSE is applied to assess collision risks and avoid obstacles.

This is without loss of generality, because the proposed work can be easily extended to articulated systems with more DOFs.

2) Regional adaptive joint constraints: During the scanning process, part of HRM's joints are located in the confined region and are constrained in mobility. Larger joints motions may lead to a collision risk, as shown in Fig. 8. Therefore, the entire HRM has two parts, one in a confined region ($J_1 - J_5$) and another in a work region ($J_6 - J_8$) based on the distribution of obstacles. The angle constraint is defined as:

$$\theta_i = \arccos \frac{\bar{P}_{i+1}\vec{P_i} \cdot \bar{P}_i P_{i-1}\vec{}}{|\bar{P}_{i+1}\vec{P_i}||\bar{P}_i P_{i-1}\vec{}|}, \quad \theta_i \in [0, \lambda\hat{\theta}] \tag{16}$$

where θ_i is the angle of joint i, $\hat{\theta}$ is the physical limits of joints, λ is the weight coefficient to regulate the joint angle changes among configurations. Adaptive weights based on spatial regions are applied to joint angle constraints. In the confined region, joint movements are restricted to small angular changes to ensure safety. In the working region, greater joint mobility is permitted to support scanning operations.

IV. Simulations and Experiments

This section presents the verification of the proposed method by performing numerical simulations and experiments, where the HRM operates within a narrow-space environment with densely packed obstacles. A video clip of our simulations and experiments can be seen from [26].

A. Numerical simulation

1) Analysis of 3DSE characteristics: In Section III, 3DSE's parameterized expression has been given for the first time to study the additional collision areas, which is defined as the area generated by the deviation of the original trajectory during HRM's movement. According to (10), 3DSE's shape depends on the configuration deflection angle α and link length L_D.

As shown in Fig. 9(a), α is set to 0°, 30°, 60°, and 90° with L_D fixed at $100mm$. As the deflection angle α increases, the additional collision area is expanded gradually. The Hausdorff distance [27] L_H is applied to evaluate the positional deviation between 3DSE and the configuration. Fig. 9(b) shows the mapping relationship between L_H and α. Correspondingly, an increase in 3DSE distance deviation leads to a significant increase in collision risk during the tracking motion.

Similarly, as shown in Fig. 9(c), L_D is set to $80mm$, $100mm$, $120mm$, and $140mm$ with α fixed at 60°. Fig. 9(d) shows the linear mapping relationship between L_H and L_D. Therefore, it is crucial to choose the appropriate length of HRM's link in narrow environments.

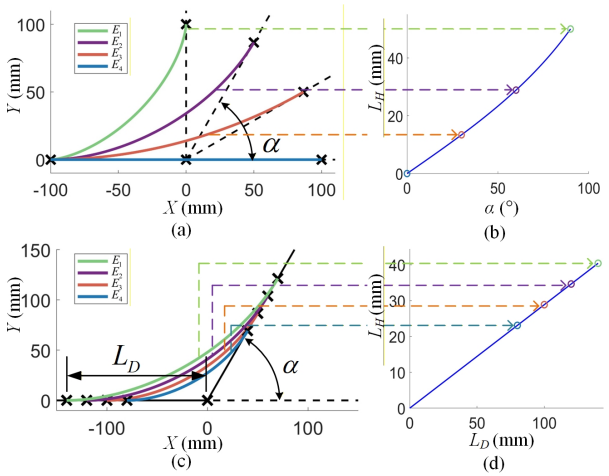

Fig. 9. Simulations of 3DSE characteristics. (a) Shape characteristics of 3DSE changing with α. (b) The Hausdorff distance changing with α. (c) Shape characteristics of 3DSE changing with L_D. (d) The Hausdorff distance changing with L_D.

2) Simulation of trajectory tracking of sinusoidal curve: To validate the advantages of proposed 3DSE method, trajectory tracking of a sinusoidal curve is simulated. As shown in Fig. 10(a), we have:

$$y = A_c \sin(w_c x + \phi_c), \tag{17}$$

where amplitude A_c is set as 83.3, frequency w_c is set as $\frac{\pi}{600}$ and phase $\phi_c = 0$. $L_D = 128.5mm$, the same as our designed prototype. Key path nodes are obtained by sequential interpolation and HRM's configuration fitting methods.

A common collision evaluation method involves proportionally expanding the tracked trajectory and constructing a virtual guiding pipeline [27]. Therefore, by calculating the Hausdorff distances of 3DSE between each pair of path nodes, the maximum value L_H determines the radius of the virtual guiding pipeline. As shown in Fig. 10(a), the virtual guiding pipeline-based method sacrifices larger free space than our proposed 3DSE-based method. The trajectory tracking process is shown in Fig. 10(b). Fig. 10(c) shows the joint angle θ_{pi} ($i \in [1, 8]$) changes during the tracking process, where d_B is the movement distance of HRM's base. Joint angle changes exhibit similar curves of variation. It indicates that by employing our proposed sliding window based tracking method, the motion of subsequent joints follows the motion pattern of the end joint. The path deviation $\tilde{L}$ during the tracking process is shown in Fig. 10(d). Except for the path deviation generated when HRM starts tracking from a horizontal configuration, the remaining process allows HRM to fit the sinusoidal curve.

3) Simulation of 3DSE-based collision avoidance: To verify the effectiveness of our proposed 3DSE-based collision avoidance algorithm, a confined space with several cylindrical obstacles is chosen as the simulation environment, as shown in Fig. 11. The initial coordinate of HRM's base is set to $(0, 0, 0)$ and the position of target point is set to $(2050, 0, 0)$. For each cylindrical obstacle, the dimension is set to $80mm$.

As shown in Fig. 11(a), the expansion size of each obstacle is set to $50mm$, the same as the dimension of HRM's link. When obstacles are expanded with such methods as [12], [13], no available space exists for HRM to pass through. In

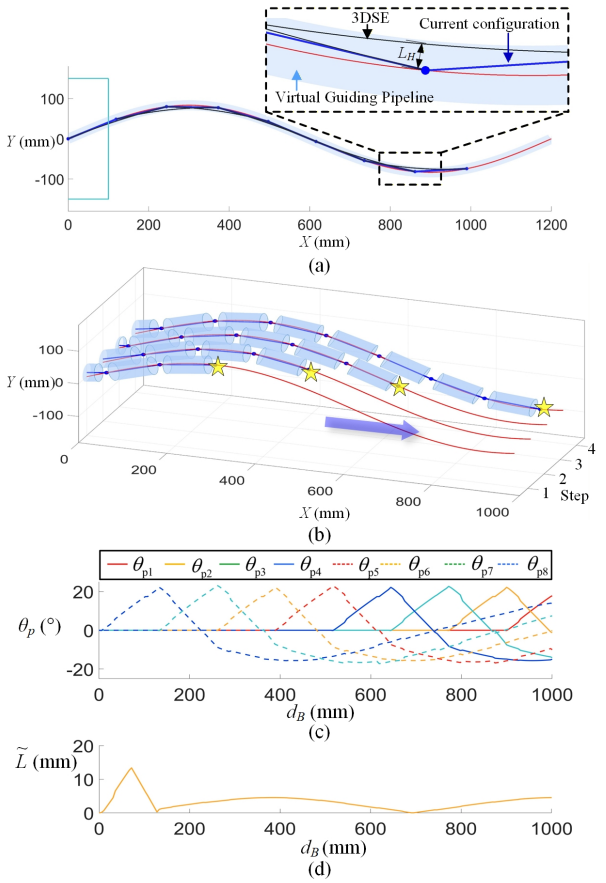

Fig. 10. Simulation of trajectory tracking of sinusoidal curve. (a) Comparison between the virtual guidance pipeline-based method [27] and 3DSE-based method. (b) Tracking process. (c) The variation in joint angles during the movement. (d) Path deviation changes during the movement.

TABLE III
INFLUENCE OF DIFFERENT PARAMETERS ON THE IK SOLUTION

$D(mm)$	i			$t(\times 10^{-4}s)$		
	$\theta_c = 60°$	40°	20°	60°	40°	20°
10	2	3	5	0.299	1.092	0.716
1	5	5	8	0.227	0.720	0.931
0.1	7	8	12	0.292	0.694	1.299
0.01	9	10	16	0.748	0.891	1.619
0.001	12	13	20	0.474	1.170	2.220

contrast, our proposed method performs trajectory planning successfully. The trajectory is updated by employing 3DSE to assess collision risks, as shown in Fig. 11(b). The path length is 1117.81mm while the obstacles are expanded and it reduced to 985.57mm by our method. The movement of HRM is kept within the green envelope. Fig. 11(c) shows the trajectory tracking process based on our sliding window method. In confined environments, HRM is able to precisely avoid obstacles and reach the target position. The joint angle changes during the tracking process is shown in Fig. 11(d).

4) Simulation of heuristic serpentine scanning: Obtaining a reliable IK solution is a prerequisite to perform blade scanning. As shown in Fig. 12, we need to compute its configuration when HRM's end-effector is located at the target position.

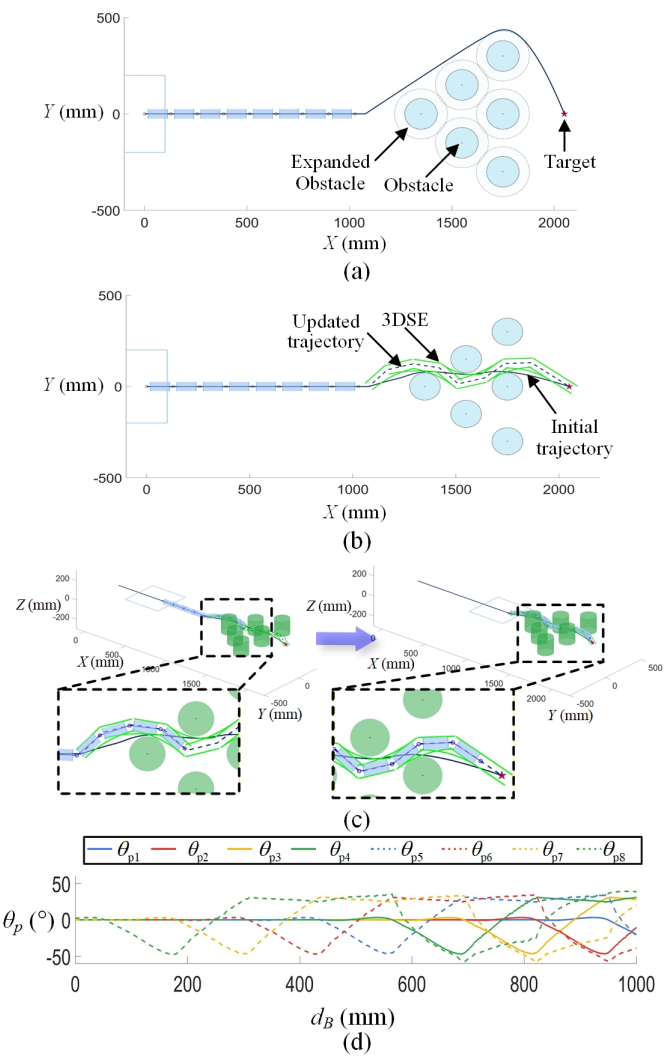

Fig. 11. Simulation of 3DSE-based collision avoidance algorithm. (a) Trajectory obtained based on expanded obstacle method. (b) Trajectory obtained based on our proposed method. (c) Tracking process. (d) Joint angles during the tracking motion.

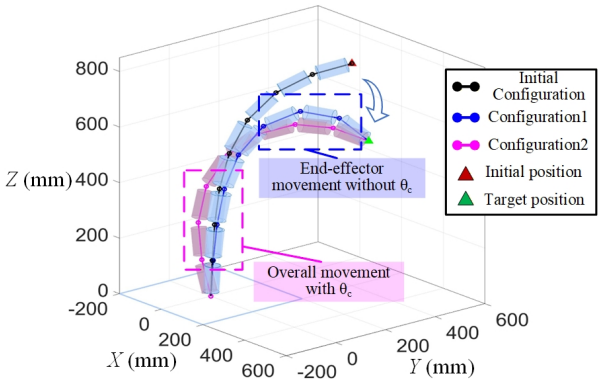

Fig. 12. Simulation of heuristic IK solution.

Configuration 1 is obtained in the absence of joint constraint θ_c, which is defined as the maximum value of joint angles $\theta_i, i \in \{1, 2, ..., 16\}$. In this case, the variation in the joint angles of HRM is primarily concentrated in the end part. Configuration 2 is obtained when θ_c is set to 20°. In this case, HRM cannot perform large-scale bending motion. Therefore, the desired configuration can be obtained by applying different

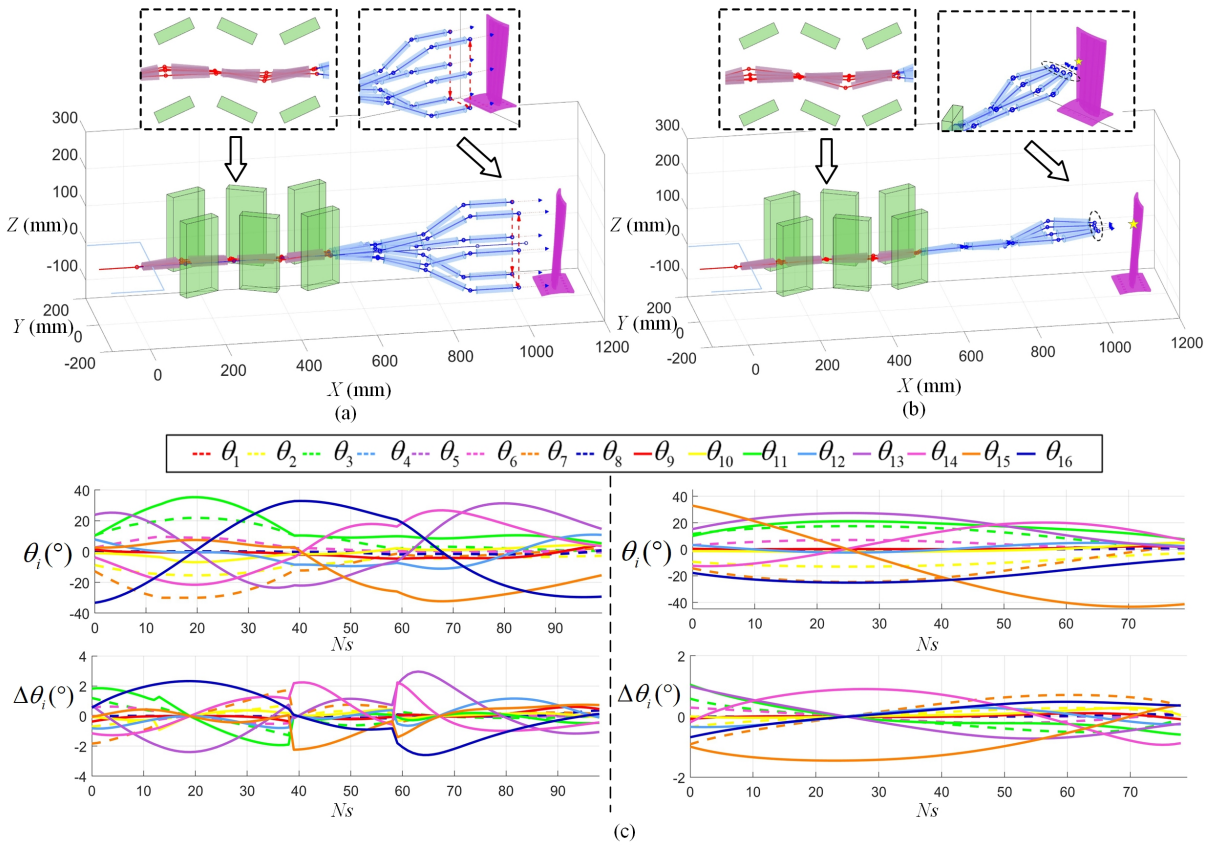

Fig. 13. Simulation of heuristic serpentine scanning. (a) Vertical scanning mode. (b) Surround scanning mode. (c) The variation in joint angles and joint angle offsets during the scanning process.

joint constraints.

The influence of different parameters on the IK solution is illustrated in Table. III. The convergence thresholds D is defined as the target value during the iteration process of our heuristic algorithm. D is set to $\{10mm, 1mm, 0.1mm, 0.01mm, 0.001mm\}$, and θ_c is set to $\{60°, 40°, 20°\}$. When the convergence threshold decreases, the number of iterations i and the corresponding calculation time t increase. The calculation time meets the real-time requirements. It should be noted that smaller θ_c may lead to the failure of IK solutions.

To satisfy the requirements of practical scanning tasks, both position and orientation of the HRM's end-effector must be considered in IK solutions. As shown in Fig. 13(a), the blade surface is scanned by using a vertical scanning mode, where the end effector orientation of HRM is perpendicular to the scanning path. The first four joints are located in confined areas and θ_c of each joint is set to 30°. The last four joints are located in free areas and θ_c of each joint is set to 45°. The convergence threshold is set to $0.001mm$.

As shown in Fig. 13(b), when blade damage is detected, the scanning mode is switched to surround scanning mode to diagnose the damage. The variation in joint angles $\{\theta_1, \theta_2, ..., \theta_{16}\}$ and the corresponding joint angle offsets $\{\Delta\theta_1, \Delta\theta_2, ..., \Delta\theta_{16}\}$ are illustrated in Fig. 13(c), where N_s represents the step count during this process.

TABLE IV
MECHATRONIC PARAMETERS OF HRM

Items	Characteristics
Total DOFs	18 (16 joint DOFs + 2 mobile DOFs)
Total number of motors	26 (24 + 2)
Dimensions of HRM	Φ 100 × 1375 (mm)
Dimensions of mobile platform	726×617×273 (mm)
Maximum speed of mobile platform	0.8 (m/s)
Total mass	87.3 (kg)
Load capability	0.5 (kg)

B. Experiments

1) Experiment setup: To validate the adaptability of our proposed method, an experimental system is developed to perform in-situ maintenance tasks for aero-engines. A 16-DOF HRM prototype with a mobile platform is developed. Its parameters are listed in Table. IV.

2) Experimental results: As illustrated in Fig. 14, our proposed 3DSE-based collision avoidance method is deployed on the prototype for the narrow space crossing tasks, validating its trajectory tracking and obstacle avoidance ability. Firstly, a proportional simulation environment is established based on the actual scenario. Then, the collision-free trajectory is calculated by our method. At the same time, the angles of joints are calculated based on the current position of each joint. Through the mapping relationship between joint space and driving space, synchronous control between simulation

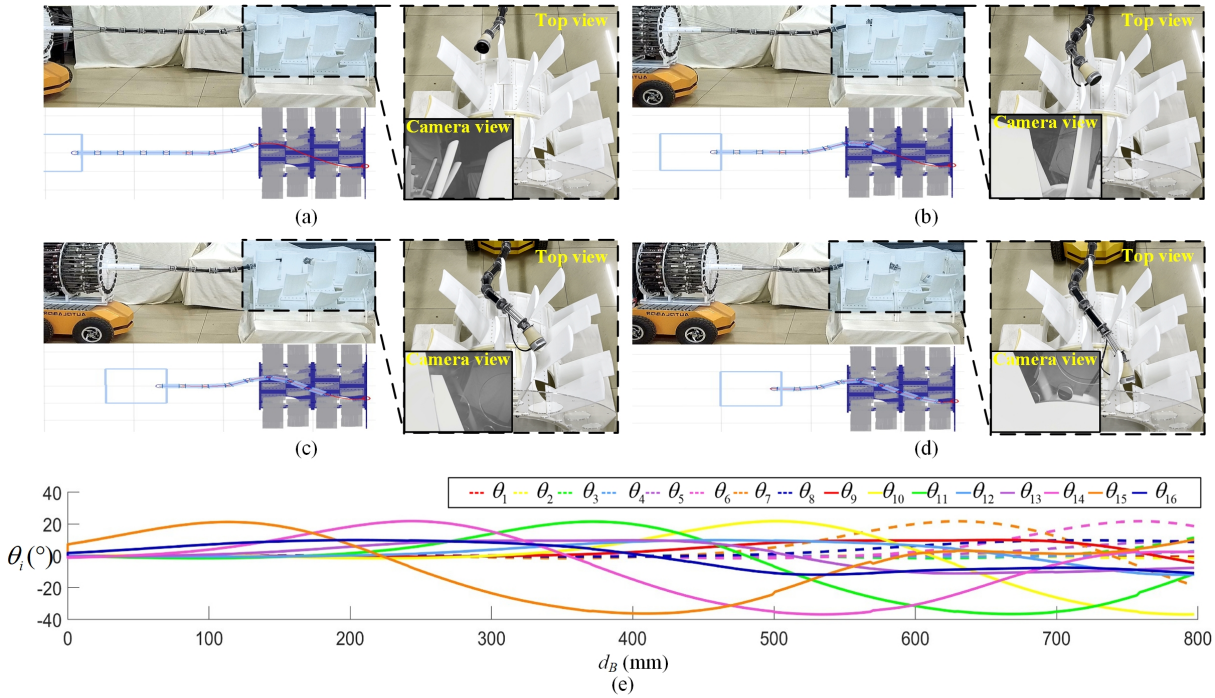

Fig. 14. Experimental results of crossing narrow areas. (a) $t = 80$s. (b) $t = 140$s. (c) $t = 180$s. (d) $t = 200$s. (e) The variation in joint angles during the crossing process.

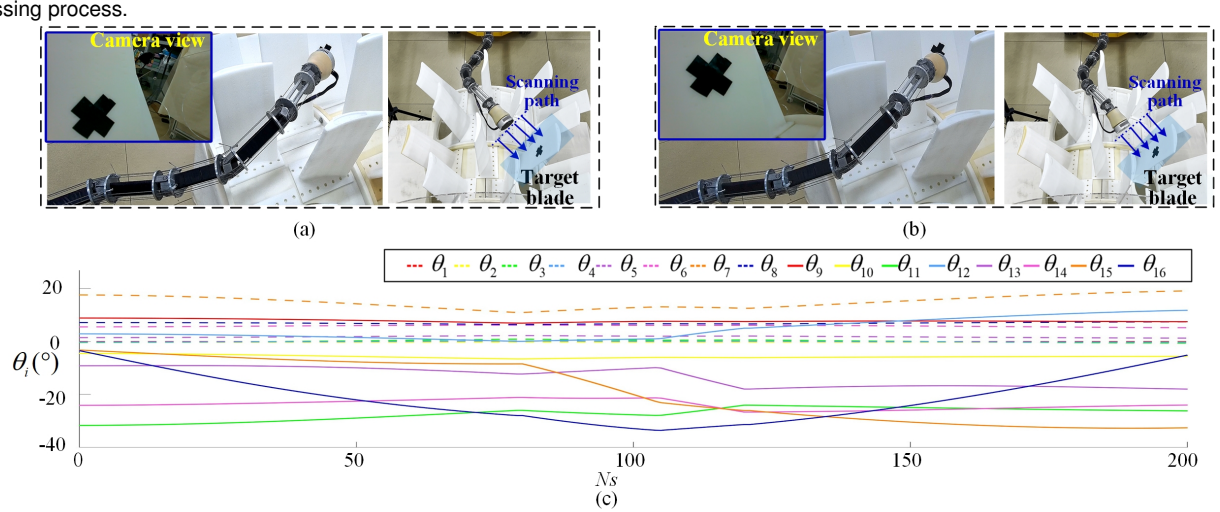

Fig. 15. Experimental results of scanning the target blade. (a) $t = 10$s. (b) $t = 20$s. (c) The variation in joint angles during the scanning process.

and the prototype is achieved. During the trajectory tracking process, angle changes are illustrated in Fig. 14(e).

Upon detecting damage during the motion through the multi-layer blade region, the next step is to perform a heuristic serpentine motion based scanning operation on the target blade. As shown in Fig. 15, HRM scans the blade and acquires image data of the damaged areas. The angle changes are shown in Fig. 15(d).

Experimental results show that HRM can move flexibly and smoothly during the traversing and inspection inside the multi-layer blade region, which indicates the effectiveness and adaptability of our proposed method. Moreover, this not only illustrates the unique advantage of our method but also shows cases its promising application potential.

V. Conclusion and Future Work

Conclusion: This work proposes a 3DSE-based motion control strategy for HRMs. 3DSE is firstly proposed to establish the collision constraints. During the trajectory tracking process, 3DSEs are applied to optimize collision-free trajectory by evaluating collision risks. To perform blade detection tasks, a heuristic serpentine scanning method based on regional adaptation is proposed after HRM reaches the target area. Simulations and experiments are implemented to verify the performances of our strategy.

Limitations and future work: However, a main limitation of this work is the lack of adaptability to uncertain environments. To achieve real-time trajectory optimization and control in dynamic scenarios, we plan to integrate 3DSE with multidimensional sensor data. Our future work aims to further improve the adaptability and reliability of proposed

algorithm by enhancing the HRM's perception capability [28]–[30]. Furthermore, intelligent optimization algorithms and generative pre-trained transformer based technologies should be employed to enhance the quality of generated paths, enabling HRMs to perform in-situ aero-engine maintenance tasks [31]–[35].

REFERENCES

[1] I. Walker, H. Choset, and G. Chirikjian, "Snake-like and continuum robots," *Springer Handbook of Robotics*, DOI 10.1007/978-3-319-32552-1_20, 2016.

[2] M. Hwang and D. Kwon, "K-FLEX: A flexible robotic platform for scar-free endoscopic surgery," *The International Journal of Medical Robotics and Computer Assisted Surgery*, vol. 16, no. 2, p. e2078, 2020.

[3] C. Lauretti, T. Grasso, E. de Marchi, S. Grazioso, and G. di Gironimo, "A geometric approach to inverse kinematics of hyper-redundant manipulators for tokamaks maintenance," *Mechanism and Machine Theory*, vol. 176, p. 104967, 2022.

[4] Z. Mu, T. Liu, W. Xu, Y. Lou, and B. Liang, "Dynamic feedforward control of spatial cable-driven hyper-redundant manipulators for on-orbit servicing," *Robotica*, vol. 37, no. 1, pp. 18–38, 2019.

[5] Z. Yang, L. Yang, Y. Sun, and X. Chen, "A novel contact-aided continuum robotic system: Design, modeling, and validation," *IEEE Transactions on Robotics*, vol. 40, pp. 3024–3043, 2024.

[6] R. Buckingham and A. Graham, "Dexterous manipulators for nuclear inspection and maintenance-case study," in *IEEE International Conference on Applied Robotics for the Power Industry*, pp. 1–6, 2010.

[7] R. Kang, Y. Guo, L. Chen, D. Branson, and J. Dai, "Design of a pneumatic muscle based continuum robot with embedded tendons," *IEEE/ASME Transactions on Mechatronics*, vol. 22, no. 2, pp. 751–761, 2017.

[8] C. Yang, S. Geng, I. Walker, D. Branson, J. Liu, J. Dai, and R. Kang, "Geometric constraint-based modeling and analysis of a novel continuum robot with shape memory alloy initiated variable stiffness," *The International Journal of Robotics Research*, vol. 39, no. 14, pp. 1620–1634, 2020.

[9] T. Liu, W. Xu, T. Yang, and Y. Li, "A hybrid active and passive cable-driven segmented redundant manipulator: Design, kinematics, and planning," *IEEE/ASME Transactions on Mechatronics*, vol. 26, no. 2, pp. 930–942, 2021.

[10] A. Martín-Barrio, J. Roldán-Gómez, I. Rodríguez, J. D. Cerro, and A. Barrientos, "Design of a hyper-redundant robot and teleoperation using mixed reality for inspection tasks," *Sensors*, vol. 20, no. 8, p. 2181, 2020.

[11] R. Ju, D. Zhang, J. Xu, H. Yuan, Z. Miao, M. Zhou, and Z. Cao, "Design, modeling, and kinematics analysis of a modular cable-driven manipulator," *ASME Journal of Mechanisms and Robotics*, vol. 14, no. 6, p. 060903, 2022.

[12] X. Zhang, J. Liu, and Y. Li, "An obstacle avoidance algorithm for space hyper-redundant manipulators using combination of RRT and shape control method," *Robotica*, vol. 40, no. 4, pp. 1036–1069, 2022.

[13] J. Yao and J. Zhao, "Decoupling sampling and planning frameworks for redundant manipulators motion planning under end-effector and performance constraints," *IEEE Transactions on Industrial Informatics*, vol. 21, no. 7, pp. 5492–5503, 2025.

[14] M. Luo, Y. Tian, E. Li, M. Chen, and M. Tan, "A local obstacle avoidance and global planning method for the follow-the-leader motion of coiled hyper-redundant manipulators," *IEEE Transactions on Industrial Informatics*, vol. 20, no. 4, pp. 6591–6602, 2024.

[15] A. Mohammad, M. Russo, Y. Fang, X. Dong, D. Axinte, and J. Kell, "An efficient follow-the-leader strategy for continuum robot navigation and coiling," *IEEE Robotics and Automation Letters*, vol. 6, no. 4, pp. 7493–7500, 2021.

[16] H. Wei, Y. Zheng, and G. Gu, "RRT-based path planning for follow-the-leader motion of hyper-redundant manipulators," in *IEEE/RSJ International Conference on Intelligent Robots and Systems*, pp. 3198–3204, 2021.

[17] X. Jiang, F. Yang, and S. Shi, "Design and full-link trajectory tracking control of underwater snake robot with vector thrusters under strong time-varying disturbances," *Ocean Engineering*, vol. 266, no. 3, p. 113012, 2022.

[18] C. Wang, H. Xie, and H. Yang, "An iterative path-following method for hyper-redundant snake-like manipulator with joint limits," *Industrial Robot*, vol. 50, no. 3, pp. 505–519, 2023.

[19] Y. Zhou, S. Wang, D. Huang, F. Ni, Y. Na, and H. Liu, "A direct discretization method of backbone curve for snake robots with multiple roll joints," *IEEE/ASME Transactions on Mechatronics*, vol. 30, no. 6, pp. 7043–7052, 2025.

[20] Z. Mu, L. Hao, Z. Wei, S. Zhao, Z. Wang, and Y. Li, "A spatial triarc planning method for configuration optimization of concentric cable-driven manipulators," *IEEE Transactions on Systems, Man, and Cybernetics: Systems*, vol. 53, no. 3, pp. 1822–1831, 2025.

[21] X. Xu, H. Xie, and C. Wang, "A kinematics method of hyper-redundant manipulators based on morphologic space constraints," *IEEE Transactions on Systems, Man, and Cybernetics: Systems*, vol. 53, no. 1, pp. 238–250, 2025.

[22] C. Yang, R. Kang, D. Branson, L. Chen, and J. Dai, "Kinematics and statics of eccentric soft bending actuators with external payloads," *Mechanism and Machine Theory*, vol. 139, pp. 526–541, 2019.

[23] T. Dana-Picard, "An automated study of isoptic curves of an astroid," *Journal of Symbolic Computation*, vol. 97, pp. 56–68, 2020.

[24] Y. Zhang, C. Han, W. Sun, W. Shao, and S. Bai, "Geometric-based method for regional-target coverage analysis," *IEEE Transactions on Aerospace and Electronic Systems*, vol. 53, no. 3, pp. 2252–2265, 2023.

[25] D. Zhang, Y. Gai, R. Ju, M. Zhou, and Z. Cao, "A cosine similarity based multitarget path planning algorithm for cable-driven manipulators," *IEEE/ASME Transactions on Mechatronics*, vol. 30, no. 3, pp. 2379–2388, 2025.

[26] "https://youtu.be/6b5awneaszu."

[27] N. Bu, N. Luo, C. Liu, Y. Sun, and Z. Xiong, "A novel path following method based on whole-body deviation evaluation for hyper-redundant robots," *IEEE Robotics and Automation Letters*, vol. 10, no. 1, pp. 604–611, 2025.

[28] F. Aimedee, G. Gogu, J. Dai, C. Bouzgarrou, and N. Bouton, "Systematization of morphing in reconfigurable mechanisms," *Mechanism and Machine Theory*, vol. 96, pp. 215–224, 2016.

[29] T. Sun, S. Yang, T. Huang, and J. Dai, "A way of relating instantaneous and finite screws based on the screw triangle product," *Mechanism and Machine Theory*, vol. 108, pp. 75–82, 2017.

[30] Z. Cao, J. Li, S. Shao, D. Zhang, and M. Zhou, "Siamese adaptive network-based accurate and robust visual object tracking algorithm for quadrupedal robots," *IEEE Transactions on Cybernetics*, vol. 55, no. 3, pp. 1264–1276, 2025.

[31] J. Li, D. Li, C. Wang, W. Guo, Z. Wang, Z. Zhang, and H. Liu, "Active collision avoidance for teleoperated multi-segment continuum robots toward minimally invasive surgery," *The International Journal of Robotics Research*, DOI 10.1177/02783649231220955, 2023.

[32] Z. Zhao, S. Li, M. Zhou, X. Li, and X. Yang, "Lexicographic dual-objective path finding in multi-agent systems," *IEEE Transactions on Automation Science and Engineering*, vol. 22, pp. 6223–6233, 2024.

[33] M. Zhou, M. Cui, D. Xu, S. Zhu, Z. Zhao, and A. Abusorrah, "Evolutionary optimization methods for high-dimensional expensive problems: A survey," *IEEE/CAA Journal of Automatica Sinica*, vol. 11, no. 5, pp. 1092–1105, 2024.

[34] Y. Liu, Y. Wen, L. Yang, L. He, and M. Zhou, "A general framework for efficient medical image analysis via shared attention vision transformer," *IEEE Transactions on Medical Imaging*, DOI 10.1109/TMI.2025.3644949, 2025.

[35] P. Lu, H. Xu, and B. Hu, "A transformer optimized planner for autonomous vehicle on-ramping merging task," *IEEE Transactions on Industrial Electronics*, vol. 72, no. 12, pp. 14 437–14 447, 2025.

Renjie Ju received the B.S. degree from the College of Information Science and Technology, Beijing University of Chemical Technology, Beijing, China, in 2018. He is currently pursuing the Ph.D. degree with the College of Information Science and Technology, Beijing University of Chemical Technology, Beijing, China. His interests include designing and optimal control of cable-driven manipulators.

Dong Zhang (S'19-M'20) received the B.S. degree from the University of Jinan, Jinan, China, in 2015, and the Ph.D. degree from the Beijing University of Chemical Technology, Beijing, China, in 2020.

He is currently an associate professor with the College of Information Science and Technology, Beijing University of Chemical Technology, Beijing. His interests include control of robots.

Yebin Wang (S'06-M'09-SM'16) received the B.Eng. degree in mechatronics engineering from Zhejiang University, Hangzhou, China, in 1997, the M.Eng. degree in control theory and control engi neering from Tsinghua University, Beijing, China, in 2001, and the Ph.D. degree in electrical engineering from the University of Alberta, Edmonton, AB, Canada, in 2008.

He has been with Mitsubishi Electric Research Laboratories, Cambridge, MA, USA, since 2009, where he is currently a Senior Principal Research Scientist. His interests include nonlinear control and estimation, optimal control, and their applications.

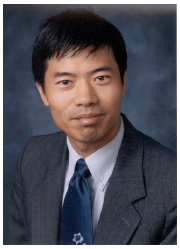

MengChu Zhou (S'88-M'90-SM'93-F'03) received his Ph. D. degree from Rensselaer Polytechnic Institute, Troy, NY in 1990 and then joined New Jersey Institute of Technology where he has been Distinguished Professor since 2013. His interests are in Petri nets, automation, robotics, big data, Internet of Things, cloud/edge computing, and AI. He has 1400+ publications including 18 books, 900+ journal papers (700+ in IEEE Trans.), 32 patents and 32 book-chapters. He is Fellow of IFAC, AAAS, CAA and NAI.

Zhengcai Cao (M'17-SM'20) received the B.S. degree in automation from the Heilongjiang University of Science and Technology, Harbin, China, in 1996, and the M.S. degree in electrical engineering and the Ph.D. degree in mechatronic engineering from the Harbin Institute of Technology, Harbin, in 2001 and 2005, respectively.

From 2008 to 2023, he is a Professor the Beijing University of Chemical Technology, Beijing, China. In 2024, he became a permanent research staff in State Key Laboratory of Robotics and Systems, Harbin Institute of Technology. His interests include system engineering and intelligent control.